6th European Conference on Computational Mechanics (ECCM 6)
7th European Conference on Computational Fluid Dynamics (ECFD 7)
11 – 15 June 2018, Glasgow, UK

NUMERICAL AND EXPERIMENTAL INVESTIGATION OF VIOLENT SLOSHING UNDER ROLL EXCITATION

RONJA HOCH [1], MATTHIAS WITTE [2] AND FRANK-HENDRIK WURM [3]

[1] ronja.hoch@uni-rostock.de

[2] matthias.witte@uni-rostock.de

[3] hendrik.wurm@uni-rostock.de

[1,2,3] University of Rostock, Albert-Einstein-Str. 2, 18059 Rostock, Germany
www.itu.uni-rostock.de

Key words: Validation, Multiphase flows, Sloshing, URANS.

Abstract. The scope of this paper is to examine sloshing with high amplitude, off-resonant roll excitation in a rectangular tank. A commercial CFD code with a homogenous multiphase model and VOF interface capturing approach is used to simulate the liquid motion. The results are validated by an experimental setup including piezoelectric pressure sensors and optical investigation of the flow. This comprises a qualitative observation of the free surface and an evaluation of the velocity field by means of an optical flow based in-house code. Whereas the pressure peaks are underestimated by the simulation, there is good agreement in the position of the liquid surface and the prediction of typical flow phenomena like wave overturning.

1 INTRODUCTION

The motion of liquid with a free surface in partially filled tanks due to external excitation is known as sloshing. It can be observed at a wide range of applications, comprising marine operations as well as automotive or spacecraft tanks [1, 2]. Automotive coolant or fuel tanks are typically exposed to high amplitude excitations due to driving manoeuvres as braking or going round bends. Sloshing liquid causes high impact pressure on the tank walls as well as air entrainment due to breaking and overturning waves. If the air is carried along into the coolant circuit or fuel supply it will cause severe damage to the engine. In order to prevent this and ensure sufficient liquid flow at the same time, various tank geometry modifications have been developed in the past. To avoid time consuming experimental test with manifold prototypes, numerical simulation of the sloshing flow is used to predict the motion of the liquid surface and entrapped air. For first test runs, the tank is assumed closed with no flow into or out of the system. Over the last decades, several approaches to investigate sloshing phenomena have been developed. While analytical methods are applicable only to a limited class of tank shapes like rectangular tanks [3], numerical methods feature a more general approach. To simulate sloshing motions, meshfree methods like smoothed particle hydrodynamics [4] as well as boundary element [5], finite difference [6] or finite volume method [7] are used. Methods based on potential theory can be used to simulate linear and nonlinear sloshing very well for many cases

[8,9]. However, they are not able to capture certain effects like wave overturning or breaking, that are typical for violent sloshing. Furthermore, dissipative effects due to damping devices are difficult to predict as the fluid is taken as inviscid.

If the Navier-Stokes equations are solved with numerical methods (CFD), it is possible to take this effects into account. In [10] sway-induced sloshing in a rectangular tank was investigated by the use of the commercial CFD solver CFX-5. Comparing a homogeneous and inhomogeneous multiphase model, they observed good agreement between inhomogeneous computational results and experimental pressure data.

In a study on the effects of turbulence model and free surface capturing methods on sloshing simulation results, [11] found out that the turbulence modelling had great influence on pressure impacts and free surface deformation whereas the choice of interface tracking model played only minor role in sloshing prediction. The LES model corresponded most closely to the experimental results compared with laminar assumption, RANS and VLES. However, [12] observed that the open-source finite difference CFD solver REEF3D, which uses the RANS approach, predicts the sloshing waves with good accuracy. The numerical results were compared to the experimentally determined free-surface elevation, which was measured using an ultrasonic sensor. Other typical methods to investigate the liquid surface elevation are wave gauges (capacitance probes) as used in [13], which only provide single point data, or camera footage that allows temporal and spatial resolution of the free surface deformation. In [14] a method to determine the surface displacement in PIV images using intensity gradients is developed. PIV or intensity gradients, as used in optical flow methods, are typically applied in the investigation of velocity flow fields as used in [15].

Most of the studies regarding sloshing are conducted for harmonic tank excitation close to the natural frequency of the liquid. Characteristic excitation amplitudes for roll motion are found in the range of 1 to 5°, for sway or surge motion they can be found at about 1 to 5% of the tank length. The maximum amplitudes found in recent publications reach 50% of the tank length [16] or 8° [17]. The tank in the present study was designed to examine flow in automotive coolant tanks and therefore the excitation differs from other studies, that typically base on marine applications. The tank is subjected to an almost harmonic roll motion with a period T_0 of 2 s and an amplitude of 45° to model accelerations up to 1 g. Amplitudes at this dimension were not found in previously published studies. The flow in a rectangular tank with and without baffles is investigated numerically and the results are compared to experimental data which comprises observation of the position of the liquid surface, magnitudes of pressure impacts and the velocity field of the flow. For the numerical simulation an URANS k-ε-model is chosen, as violent sloshing with breaking waves is expected.

2 COMPUTATIONAL MODELLING

2.1 Governing equations

In the following section the governing equations and the numerical setup used in this study are presented. To solve the equation system the numerical solver ANSYS CFX 15.0 is used. A homogenous multiphase model was chosen, to enhance speed and stability of the simulation process and make it applicable not only for academic research but also for industrial application. The homogenous model assumes that both phases, water and air, denoted as α and β, share a common flow field so that, with exception of volume fraction, only bulk transport equations

have to be solved. The conservation of mass for phase α can be described as

$$\frac{\partial}{\partial t}(r_\alpha \rho_\alpha) + \frac{\partial}{\partial x_i}(r_\alpha u_i) = m + \Gamma_{\alpha\beta}. \tag{1}$$

Here r_α represents volume fraction and ρ_α density of phase α, u_i is the flow velocity. The terms m and $\Gamma_{\alpha\beta}$ stand for mass sources and interphase mass transfer that were neglected. The momentum transport equation is given by

$$\frac{\partial}{\partial t}(\rho u_i) + \frac{\partial}{\partial x_i}(\rho u_i u_j) = -\frac{\partial p}{\partial x_i} + \frac{\partial \tau_{ij}}{\partial x_j} + b_i \tag{2}$$

where b_i represent body forces and τ_{ij} is a stress tensor that can be expressed as

$$\tau_{ij} = \mu\left(\frac{\partial u_j}{\partial x_i} + \frac{\partial u_i}{\partial x_j}\right) \tag{3}$$

The momentum transport equation uses bulk fluid properties for density ρ and viscosity μ which are defined as

$$\rho = \sum_{\alpha=1}^{2} r_\alpha \rho_\alpha \tag{4}$$

and

$$\mu = \sum_{\alpha=1}^{2} r_\alpha \mu_\alpha \tag{5}$$

2.2 Numerical setup

The governing equations (1), (2) are discretized using the finite volume method. The computational grid generated for the tank without baffles comprises 650 000 hexahedral elements, with a mean element size of 1.6 mm and the first node offset 0.8 mm from the wall. To assure grid independence of the results, maximum pressure peaks at different points are compared to those of a coarser grid as well as a finer one (2 350 000 elements). The results are presented in Table 1.

Table 1: Results of the grid independence study.

Grid elements	Difference relative to the finest grid		
	p1	p2	p3
260 000	0.91%	0.85%	0.09%
650 000	0.15%	0.71%	0.07%

It's apparent that there is only small deviation between the finest grid and the one used in this study. Using this mesh it was possible to accomplish short computing time as well as a sufficient resolution of the liquid surface.

The turbulence model chosen for this study is the k-ε-model based on the eddy viscosity concept due to its numerical robustness. The present setup uses a high-resolution advection

scheme, a second-order backward Euler time marching scheme and a coupled volume fraction algorithm. The flow is defined as free surface flow and the time step-size is 0.001 s. For each geometry three cycles were simulated to avoid irregularities at the beginning of the motion and it appeared that the pressure data did not change after the second cycles so that only the last cycle was used for the evaluation.

3 EXPERIMENTAL FACILITIES AND PROCEDURES

The object of the experimental investigations is a modular, rectangular tank consisting of 15 mm thick transparent acrylic panels. To enable the testing of different baffle types, the internal structures are interchangeable. The tank volume resembles typical coolant tanks, so no scaling effects have to be taken into account. To measure pressure impacts, five piezo-electric pressure sensors of type 112A22 by PCB are installed at the tank bottom and side walls. In Figure 1 the inner tank dimensions and the position of pressure sensors as well as the size and positions of the baffles can be seen. The used baffles are made of acrylic panels and have a wall thickness of 3 mm. The test rig consists of the tank itself which is tilted by a rotary indexing table and a camera with a position fixed in relation to the tank to maintain a constant frame.

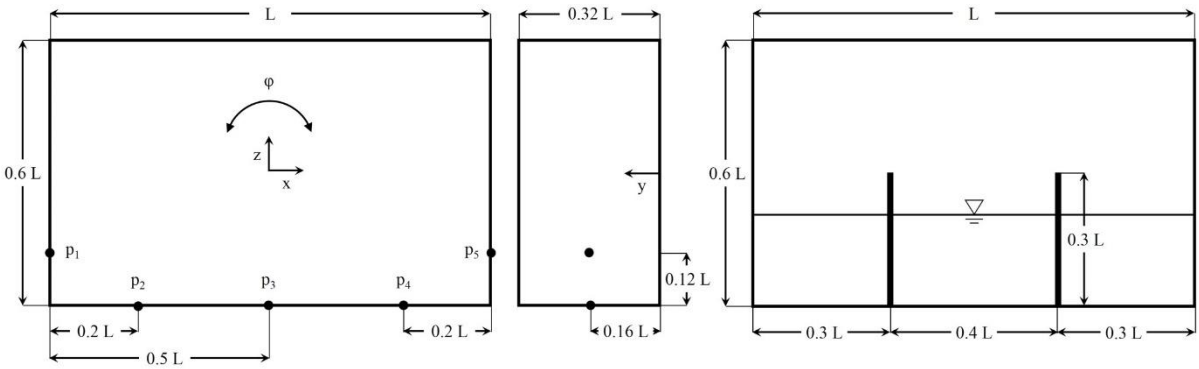

Figure 1: Dimensions of the tank and positions of pressure sensors and baffles

The rotary drive is controlled via LabVIEW and the roll angle is measured at the same time. An oscillating model acceleration profile was developed considering typical sports car acceleration profiles and then converted into a roll motion around the y-axis using the following formula:

$$\varphi = tan^{-1}\left(\frac{a}{g}\right) \tag{6}$$

where a and g represent the actual and the gravitational acceleration and φ is the equivalent angle. In Figure 2 the resulting angular excitation profile is depicted which resembles a harmonic motion. The excitation is defined by a period T_0 of 2 s and an amplitude φ_0 of 45°. This results in an angular frequency ω_0 of 3.14 rad/s.

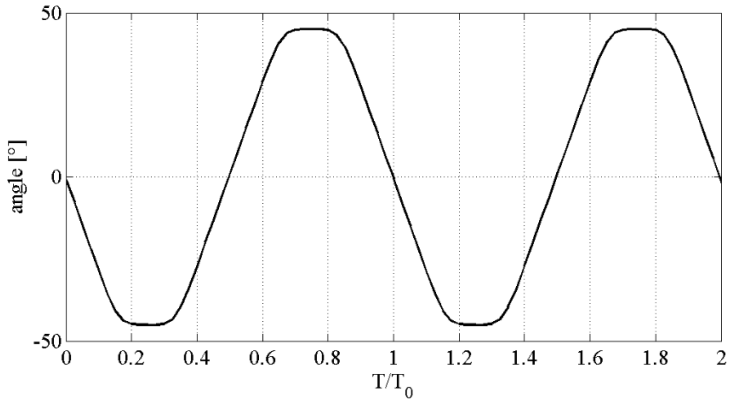

Figure 2: Roll angle of the tank over time.

The sloshing response to the excitation depends on its frequency. If the excitation frequency of the tank is in the vicinity of one of the natural frequencies of the liquid in the tank, severe sloshing is expected. The first natural frequency for a rectangular tank can be estimated by

$$\omega_n = \sqrt{\frac{\pi g}{l} tanh\left(\pi \frac{h}{l}\right)} \tag{7}$$

where l features the tank length, h represents the filling level and ω_n the first natural frequency. This formula is applicable for tanks without any baffle arrangements, because the liquid natural frequency shifts if the internal geometry is changed. For the given tank and filling level of 0.3 L the corresponding frequency is 9.53 rad/s. It is shown, that the measurements are operated at off-resonant conditions. Due to the symmetry of the excitation, only three pressure locations (p_1, p_2 and p_3) will be regarded in the results section.

For each tank configuration (without baffles and with vertical baffle arrangement) pressure data were recorded for 150 consecutive cycles with a sampling frequency of approximately 8200 Hz. The particular phase average of the last 100 measured cycles was analyzed to compare numerical and experimental results. In addition the camera recorded pictures of the flow field with a rate of 240 frames per second. The optical examination was complemented with a vertical laser sheet using a 2.5 W continuous wave laser and polyamide tracer particles to highlight and determine the position of the liquid surface and the fluid movement. For the evaluation of the particle displacements between two successive images frames an optical flow based in-house code, developed and demonstrated in [18], was used. The used optical flow approach incorporates an multi resolution and multi scale scheme to handle large particle displacements. The robust method presented in [19] was used for image regularization to assure that displacement fields are smooth and displacement gradients kept limited. The results of the validation of the numerical results will be presented in the following section.

4 RESULTS AND DISCUSSION

4.1 Wall pressures

In Figure 3 and 4 measured and calculated pressure history for both baffle configurations are presented. The pressure values were scaled by the maximum measured pressure over all sensor

points for each baffle configuration. In general, the predicted temporal distribution of pressure minima and maxima matches the pressure peaks in the experiment very well. Some minor deviations between the experiment and numerical simulation can be observed in terms of absolute pressure amplitudes and the relative phase which was observed in a similar manner in [10].

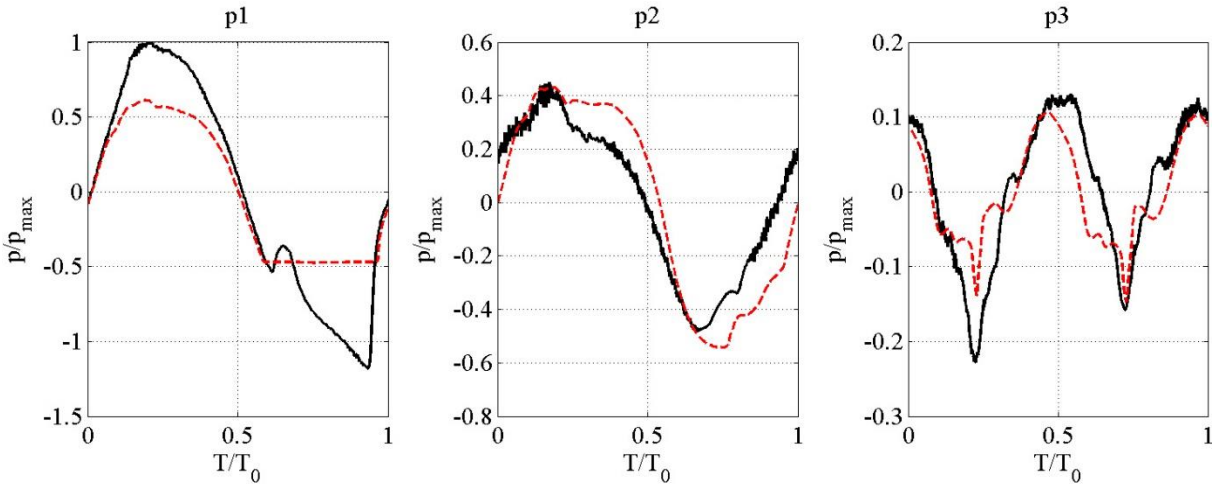

Figure 3: Pressure history at three different positions for tank without baffles (solid black line: experiment, dashed red line: simulation)

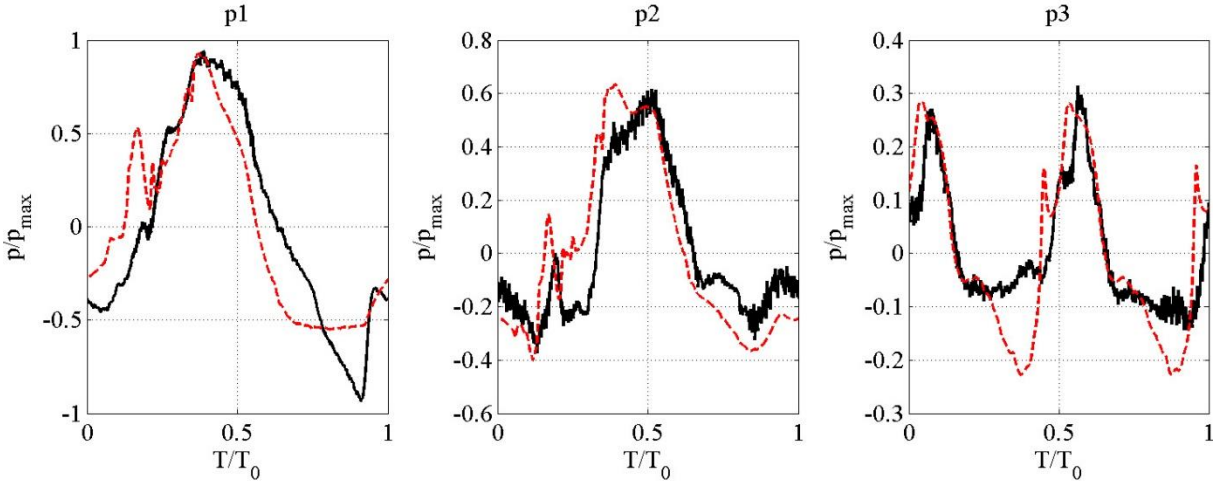

Figure 4: Pressure history at three different positions for tank with vertical baffles (solid black line: experiment, dashed red line: simulation)

Considering the measured pressure history at point p1 there is a strong decrease in the second half of the cycle from 0.7 to 0.9 T/T_0 for both baffle configurations. This occurs if the water flows away from the tank wall due to the tank movement so that for this period of time no liquid covers the sensor. While there are no hydrodynamic loads in this period, no strong pressure fluctuations should be observed. In the simulation this results in a nearly constant value because

the sensor is exposed only to atmospheric pressure, whereas in the experiments a strong pressure drop appears which seems unphysical. Similar behavior was seen in [20] for piezoelectric sensors but has not been finally clarified yet.

4.2 Motion of the free surface

To compare the displacement of the free surface directly, the free surface contour, i.e. the contour of 50% phase volume fraction derived from simulation results is plotted above camera shots of the experimental laser sheet.

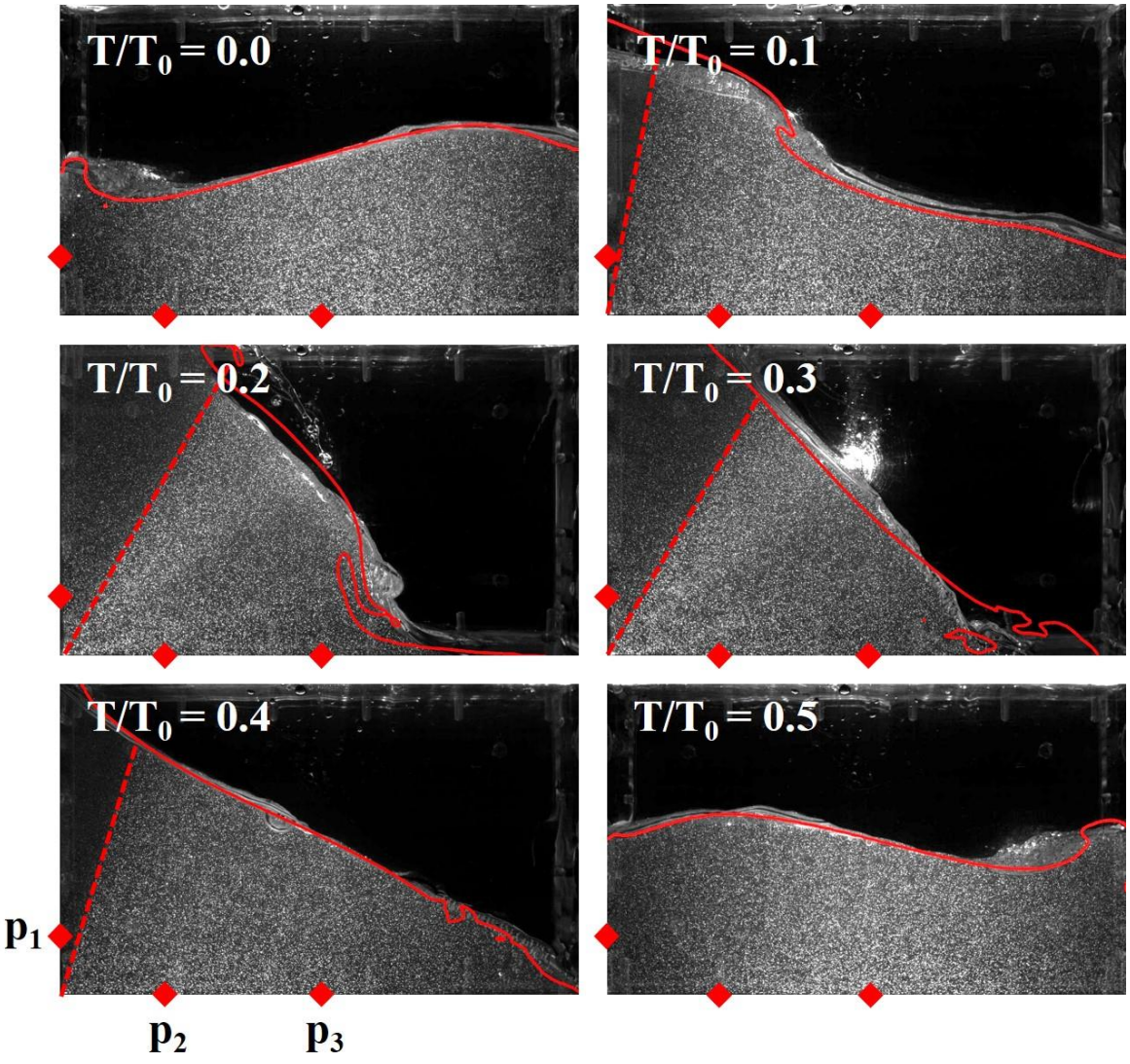

Figure 5: Evolution of free surface profile for tank without baffles. Position of pressure sensors is marked red. The solid red line represents the simulated free surface, the dashed red line marks the critical light intensity area.

Figures 5 and 6 illustrate the free surface profiles. Because the laser sheet is reflected by the tank walls at some angles, there are areas with lower light intensity. These sectors are marked

with a dashed red line in Figure 5. The simulated results correspond closely to the real behavior, even enclosed areas of air as well as overturning waves can be observed. However there are some discrepancies in the baffled tank. Whereas at $T/T_0 = 0.2$ the wall and roof impact is predicted well, at $T/T_0 = 0.3$ the flow over the left baffle and the inclination of the liquid surface seem to be overpredicted. Similar behavior can be seen at the left baffle at $T/T_0 = 0.0$ and the right baffle at $T/T_0 = 0.5$, respectively.

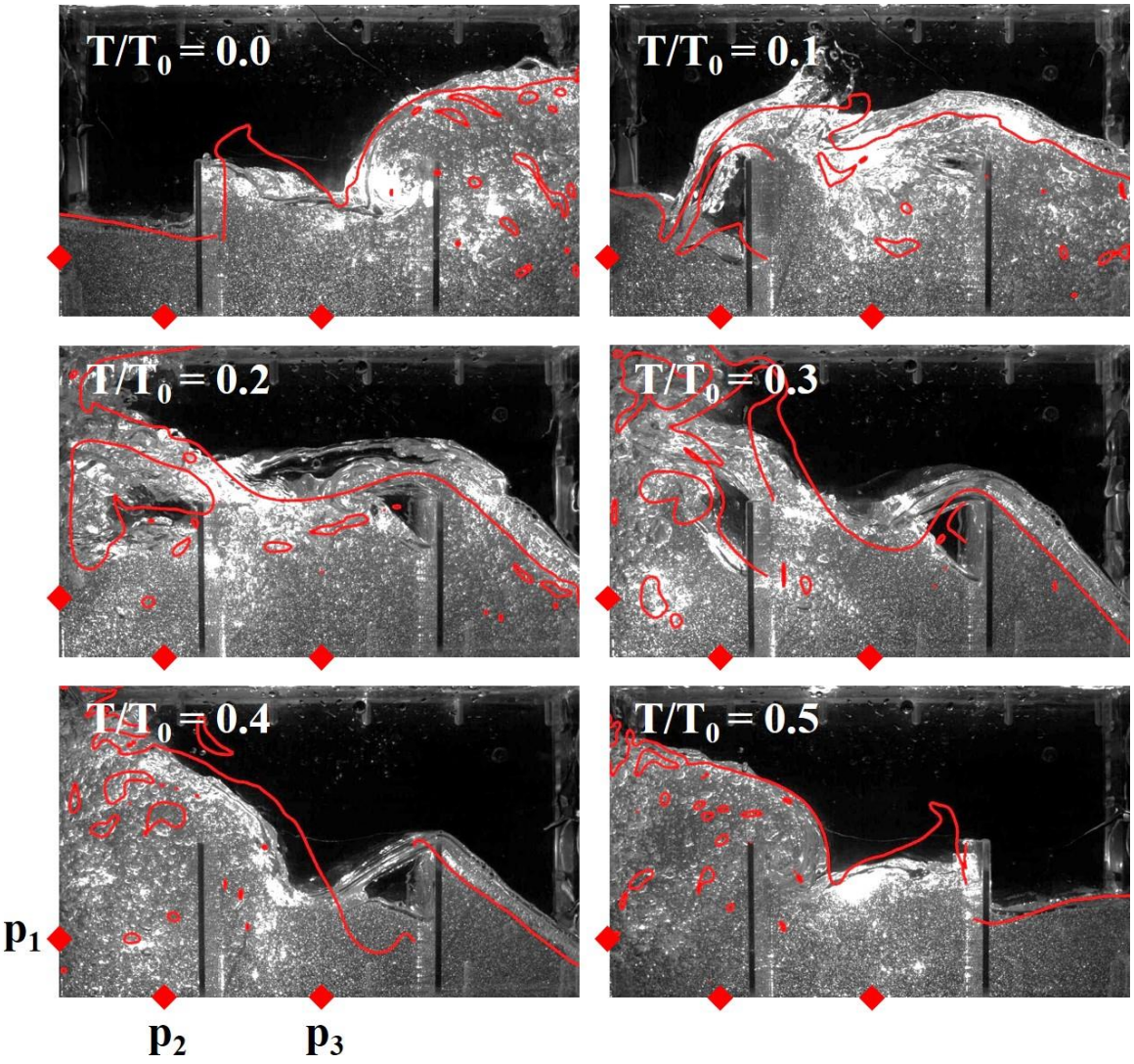

Figure 6: Evolution of free surface profile for tank with vertical baffles. Position of pressure sensors is marked red. The solid red line represents the simulated free surface.

On the other hand the flow over the right baffle at $T/T_0 = 0.4$ is not fully resolved by the simulation. This can be explained by the resolution of the computational mesh and the solver setup. The interface thickness typically spans several mesh elements as CFX does not use interface reconstruction methods. The enclosed liquid core in the case of very narrow water

streams cannot be resolved by the used mesh which was chosen for the benefit of shorter computing time. Nonetheless, regarding the prediction of phase distribution this model is suitable to predict air entrainment for design and optimization processes of coolant tanks.

4.3 Velocity field

In the following section velocity fields for the unbaffled tank will be discussed with a focus on the time around the maximum tilting angle where the most complex flow is expected. The analysis of the velocity fields within the laser light sheet was done using the optical flow approach; see [20] and [18]. As can be seen in Figure 6 the vertical baffles induce strong swirling and air entrainment. The entrapped bubbles cause strong reflections of the laser sheet and therefore disturb the evaluation of the velocity fields. The velocity values are made dimensionless using the tank length and the excitation period.

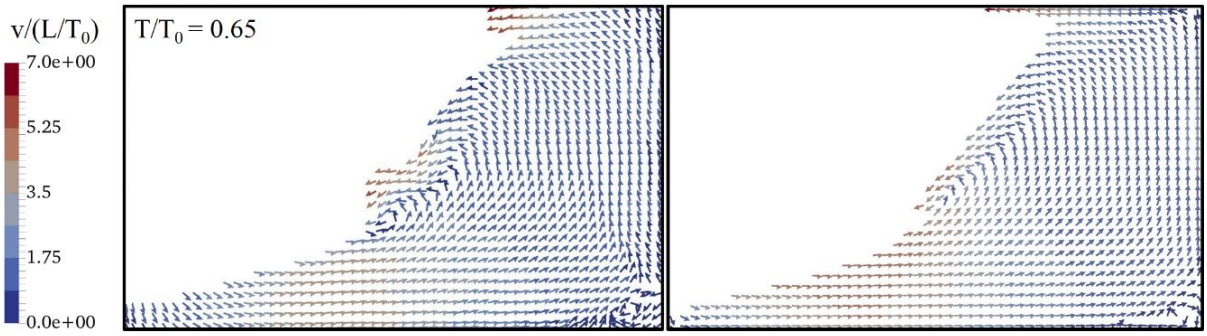

Figure 7: Velocity field for tank without baffles and $T/T_0 = 0.65$ (left: experiment, right: simulation).

Figure 7 depicts the velocity field for $T/T_0 = 0.65$ when the tank approaches the maximum tilting angle. As the water flows towards and upwards the right side of the tank, a typical vortex forms in the lower right corner of the tank because the liquid is not able to follow the sharp edge of the corner.When the liquid reaches the tank top, a water jet forms due to the high impact. Furthermore, experimental and numerical results show the overturning of the liquid front that results in a counterclockwise rotating swirl at the middle of the free surface. The flow phenomena as well as the velocity magnitudes are well predicted by the simulation.

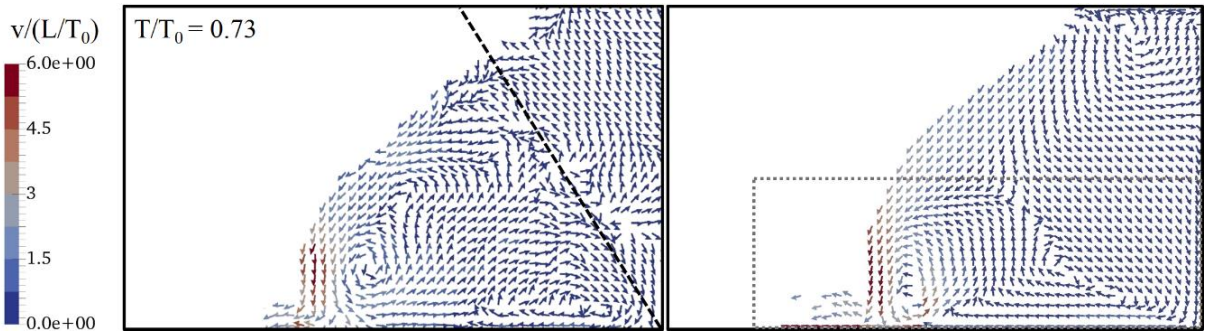

Figure 8: Velocity field for tank without baffles and $T/T_0 = 0.73$ (left: experiment, right: simulation). The dashed black line marks critical light area. The dashed gray rectangle represents the section shown in detail in Figure 9.

In Figure 8 the downstream of the liquid can be seen when the tank reaches the maximum angle. Two main flow directions can be observed: the flow at the water front that is dominated by the overturning liquid and the flow towards the lower right corner that is driven by gravity, The deflection of the water at the rigid tank walls leads to formation of vortices in the lower half of the tank which are depicted in detail in Figure 9. The locations of the vortex cores differ slightly from simulated to experimental results, but in general the flow mechanisms and velocity magnitudes are in good agreement.

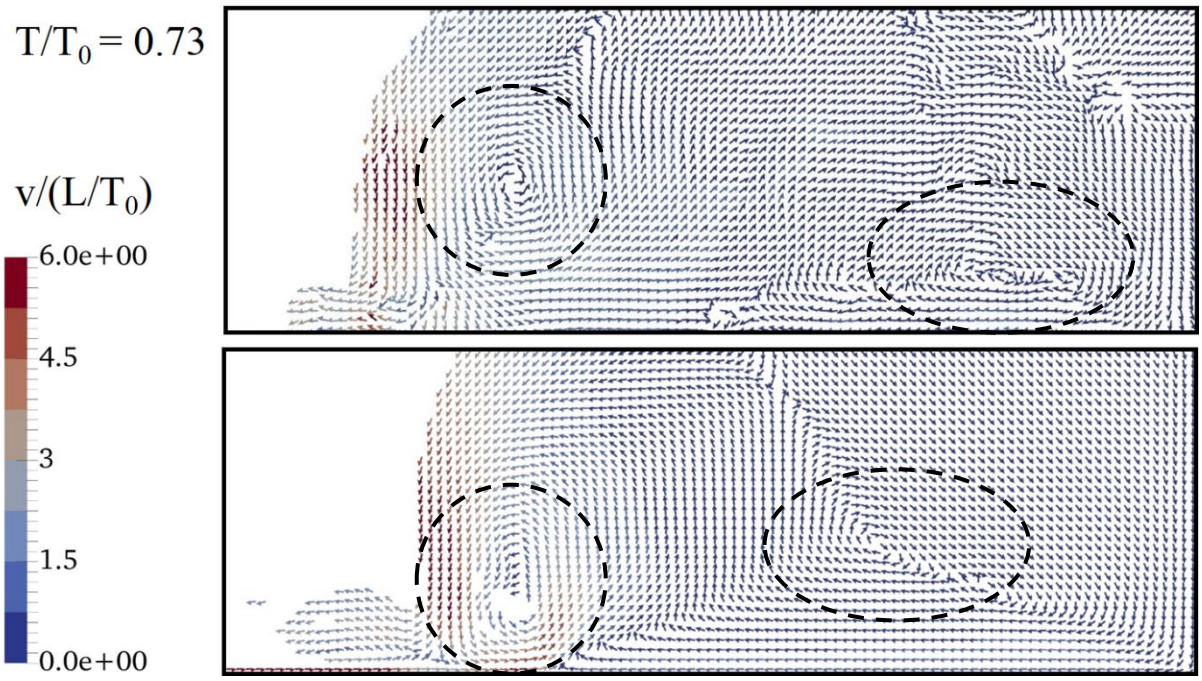

Figure 9: Detailed view of the velocity field for tank without baffles and $T/T_0 = 0.73$ (top: experiment, bottom: simulation). The dashed black line marks the vortex areas.

In the numerical results in Figure 8, a counter clockwise vortex in the upper left corner can be observed that is not captured in the experiments. The reason for this could be found in the decrease of image brightness in the top corner due to reflection at the tank walls which can be seen in Figure 5 at $T/T_0 = 0.1 – 0.4$. Because of the lower contrast of the tracer particles, the computation of particle displacment can be incorrect in this region which is marked in Figures 8 and 10 by a dashed black line.

Figure 10 displays the flow field right before the tank tilts back. Whereas the two main flow directions towards the left and right lower corners of the tank can be seen in both images, the experimental flow field shows more turbulent structures that are not found in the simulation. Near the middle of the tank bottom a structure can be seen which resembles a hydraulic jump in the numerical results and leads to a clockwise rotating swirl in the measured flow field (dashed gray line in Figure 10). The other clockwise vortex in the lower right half of the tank which is already found at $T/T_0 = 0.73$ continues in the experiments but has vanished in the simulation (solid gray line in Figure 10). This might be due to the dissipative character of the k-ε-model.

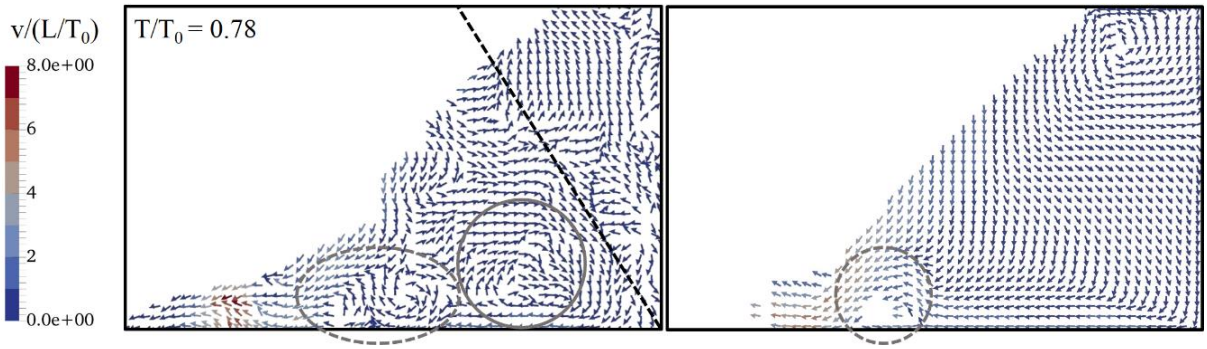

Figure 10: Velocity field for tank without baffles and $T/T_0 = 0.78$ (left: experiment, right: simulation). The dashed black line marks critical light area, the gray lines mark flow phenomena

The velocity at the wave front is underpredicted by the simulation. Again the flow structure in the upper right part of the domain was not captured satisfactorily in the experiments due to insufficient illumination.

5 CONCLUSIONS

Sloshing motion inside a rectangular tank with and without vertical baffles has been simulated numerically at exceptional high excitation amplitude and off resonant conditions to examine the applicability of the numerical code in the design and optimization process of automotive coolant tanks. As previous studies focus mostly on marine applications, the effects of high amplitude excitation were not investigated before. As a first step, the tank was considered a closed system without in- or outlets. Experiments have been conducted to validate the results regarding the pressure impacts at tank walls, position of the free surface and the velocity field. To enable numerical stability and fast computing speed, a medium mesh with element size of 1.6 mm and the k-ε turbulence model were chosen. It has been shown, that the simulation is able to predict the phase distribution and major flow phenomena like vortices sufficiently, but underestimates the pressure impacts. As wall pressures are only a minor concern in the design of coolant tanks and the main objective is to predict air entrapment, the numerical setup seems suitable for this application. In future work the interaction of flow through the tank and liquid movement due to external excitation will be examined.

REFERENCES

[1] Ibrahim, R. A. *Liquid sloshing dynamics: Theory and applications*. Cambridge University Press (2006).
[2] Faltinsen, O. M. and Timokha, A. *Sloshing*. Cambridge University Press (2009).
[3] Cho, I. H., Choi, J.-S. and Kim, M. H. Sloshing reduction in a swaying rectangular tank by an horizontal porous baffle. *Ocean Engineering* (2017) **138**:23–34.
[4] Colagrossi, A., Lugni, C. and Brocchini, M. A study of violent sloshing wave impacts using an improved SPH method. *Journal of Hydraulic Research* (2010) **48** No. **S1**:94–104.

[5] Ning, D.-Z. et al. A Boundary Element Investigation of Liquid Sloshing in Coupled Horizontal and Vertical Excitation. *Journal of Applied Mathematics* (2012) **2012** No. **1074**:1–20.
[6] Akyildiz, H. A numerical study of the effects of the vertical baffle on liquid sloshing in two-dimensional rectangular tank. *Journal of Sound and Vibration* (2012) **331** No. **1**:41–52.
[7] Yu, Y.-M. et al. Experimental and numerical studies on sloshing in a membrane-type LNG tank with two floating plates. *Ocean Engineering* (2017) **129**:217–227.
[8] Mehl, B. *Sloshing: experimentelle und theoretische Studien zum Einfluss ausgewählter Parameter auf die Wellenbewegungen in teilgefüllten Tanks*. Shaker (2015).
[9] Zhang, H. and Sun, B. Numerical Simulation of Sloshing in 2D Rectangular Tanks Based on the Prediction of Free Surface. *Mathematical Problems in Engineering* (2014) **2014** No. **4**:1–12.
[10] Godderidge, B. et al. An investigation of multiphase CFD modelling of a lateral sloshing tank. *Computers & Fluids* (2009) **38** No. **2**:183–193.
[11] Liu, D. et al. Modelling of liquid sloshing using CLSVOF method and very large eddy simulation. *Ocean Engineering* (2017) **129**:160–176.
[12] Grotle, E. L., Bihs, H. and Æsøy, V. Experimental and numerical investigation of sloshing under roll excitation at shallow liquid depths. *Ocean Engineering* (2017) **138**:73–85.
[13] Xue, M.-A. et al. Violent transient sloshing-wave interaction with a baffle in a three-dimensional numerical tank. *Journal of Ocean University of China* (2017) **16** No. **4**:661–673.
[14] Zarruk, G. A. Measurement of free surface deformation in PIV images. *Measurement Science and Technology* (2005) **16** No. **10**:1970–1975.
[15] Tanaka, G. et al. Simultaneous measurement of free-surface and turbulence interaction using specklegram method and stereo-PIV. *Applications of Laser Techniques to Fluid Mechanics*. Lisbon, Portugal.
[16] Moo Ji, Y. et al. Experiments on non-resonant sloshing in a rectangular tank with large amplitude lateral oscillation. *Ocean Engineering* (2012) **50**:10–22.
[17] Akyildiz, H. and Ünal, E. Experimental investigation of pressure distribution on a rectangular tank due to the liquid sloshing. *Ocean Engineering* (2005) **32** No. **11-12**:1503–1516.
[18] Kapulla, R. et al. Optical Flow and Cross Correlation Techniques for Velocity Field Calculation. *Lasermethoden in der Strömungsmesstechnik: 17. Fachtagung, 8. - 10. September 2009, Erlangen*. GALA, Karlsruhe (2009):6.1–7.
[19] Horn, B. K. and Schunck, B. G. Determining Optical Flow. *Artificial Intelligence* (1981) **17**:185–203.
[20] Kim, S.-Y., Kim, K.-H. and Kim, Y. Comparative study on pressure sensors for sloshing experiment. *Ocean Engineering* (2015) **94**:199–212.